DOI: 10.61782/fa.2025.0807

FORUM ACUSTICUM EURONOISE 2025

SPARSE ARRAYS FOR 3D ULTRASOUND MICROSTRUCTURE IMAGING

Óscar Martínez-Graullera[1*] **Jorge Camacho**[1] **Jorge Huecas**[1]
Guillermo Cosarinsky[1] **Luis Elvira**[1] **Alberto Ibañez**[1]
[1] Instituto de Tecnologías Físicas y de la Información (ITEFI), CSIC, Spain

ABSTRACT

In the last decade, plane-wave-based volumetric ultrasonic imaging has become a promising research tool in preclinical neuroscience. Its high-speed imaging capability at a high operating frequency allows the observation of microvascular structures and the acquisition of functional ultrasound (fUS) images. However, achieving high-quality 3D super-resolution images requires fully functional full apertures supported by many independent channels, as well as high data transmission rates and processing capacity. Based on current technology, which emulates full array performance through multiplexing, this technique is far from reaching full maturity. This study investigates the potential of sparse arrays to achieve a trade-off in designing 3D imaging systems for fUS. Starting with a 32x32-element aperture, sparse array configurations with up to 256 elements for transmission and reception are explored. The study examines the requirements and opportunities of this approach during pre-beamforming and beamforming stages, focusing on system architecture.

Keywords: *plane wave, sparse array, ultrasonic imaging, volumetric imaging.*

1. INTRODUCTION

The plane-wave imaging technique involves emitting a plane wavefront and forming the image during reception by compensating for both the distance to the receivers and the distance traveled by the wavefront during transmission [1, 2]. Because the imaging region is very close to the aperture, the plane wave itself—during its formation process—primarily generates the acoustic noise responsible for the artifacts. Although this technique produces significant sidelobes and lower-quality images, it offers the advantage of very fast acquisition, thereby enabling new applications such as functional imaging [3,4]. To improve image quality, multiple images acquired at different transmission angles are combined. The diversity in the sidelobe distribution leads to their cancellation when combined, enhancing the overall image quality. In this way, a balance between image quality and acquisition speed can be sought.

In linear arrays, the number of angles used varies depending on the required image quality, with typical values ranging from 3 to 30 angles [1]. For two-dimensional arrays, these values range from 5×5 to 11×11 angles [2]. Determining the optimal number of angles requires prior experimental validation or a simulation model to balance image quality and acquisition complexity.

Volumetric imaging remains a technological challenge [5, 6]. One major limitation is the difficulty in achieving apertures with sufficient dimensions to provide high resolution. Current models in the literature typically assume a (32×32) element array (1024 elements) with inter-element spacing exceeding $\lambda/2$. Another critical challenge is the parallel control of a large number of elements. Only recently have systems been developed that support up to 256 elements in parallel, often relying on complex setups with multiple systems to reach that number.

The quality of plane-wave imaging is achieved through diversity. A set of images where the prevalence

*__Corresponding author__: oscar.martinez@csic.es.

of reflectors against a background of varying noise from image to image enhances their presence and smooths out the sidelobes. This always occurs within a space primarily limited to the projection of the aperture—the region insonified by the plane wave—where the main contribution to the image comes from the 0-degree angle transmission, while the remaining angles provide diversity.

From the system's perspective, the ability to generate high-speed imaging depends not only on the time of flight but also on how quickly the acquisition buffers become available again (i.e., the time required to transmit the data to the storage unit). This time depends on the communication interface, for example, for an acquisition time of 14 microseconds and 256 parallel channels, it can be 150 microseconds (with a high-speed 3GBps interface) or 6.4 milliseconds (with a more common Gigabit Ethernet interface).

2. SPARSE ARRAYS FOR PLANEWAVE

For this work, we take as a reference the problem of operating a two-dimensional aperture of 1024 elements (32×32) spaced at λ at a central frequency of 15 MHz, using no more than 256 elements. This represents a 4-to-1 reduction, which can be implemented in various ways. However, when designing a sparse aperture, it is necessary to take into account the constraints imposed by the associated imaging modality. The volumetric imaging space considered ranges from 3 to 7 mm in depth, with a maximum size of 4 mm per side.

Therefore, it is important to analyze how the transmitted wavefront contributes to the generation of sidelobes in the near-field region of the aperture [7]. Figure 1 shows a representation of the wavefront generated by our reference aperture at $Z = 6mm$ in the fully populated case. The projection of the array, which is the area where the image is intended to be obtained, is marked by the two black lines. The complexity of the global wavefront pattern arises from the two-dimensional distribution of the elements, which leads to the formation of multiple secondary wavefronts, resulting in imaging artifacts. One way to mitigate these interfering wavefronts is by deactivating the outer elements.

In this case, the aperture is reduced to 256 elements—specifically, by limiting the emitting aperture to the central (16×16) elements. However, secondary lobes remain high due to the boxcar aperture shape. To reduce them, we can apply an apodization scheme based on element distribution.

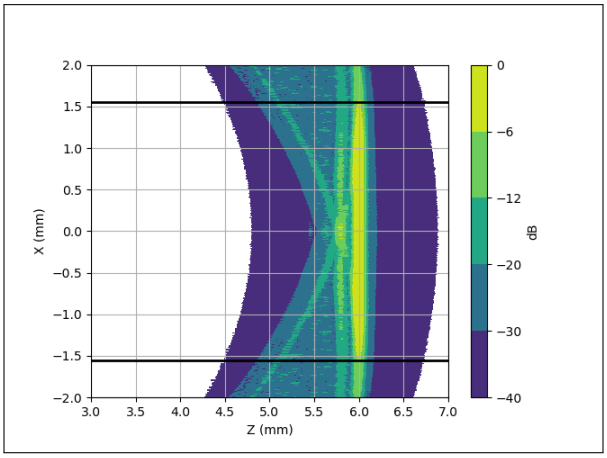

Figure 1. Emission waveform in $Y = 0$, fully populated case.

If we consider a sparse element distribution, such as a binned array, configured using a density scheme that implements a low-sidelobe window (in this case, a Taylor window), it is possible—at the cost of reducing the main wavefront size to one-third of that of the fully populated aperture—to suppress the main secondary wavefronts and reduce parasitic wavefronts to an irregular structure with very low intensity (figure 2). It is worth to mention that this apodization scheme avoids changing the emission voltage for each array element, a feature that is not available in all ultrasound systems.

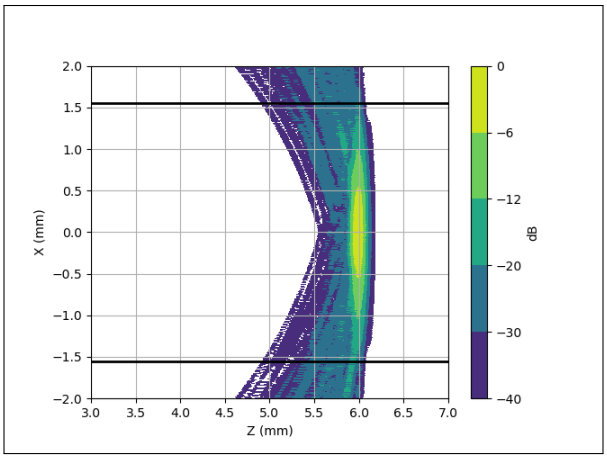

Figure 2. Emission waveform in $Y = 0$, 256 sparse case following a density apodization based on Taylor window

In reception, on the other hand, it is necessary to choose a solution that implements narrow beams to provide high-resolution imaging. In this regard, we have opted for a ring-shaped distribution. In both cases, we start by dividing the aperture into 4×4 bins, allowing us to select between 1 and 16 active elements per bin, depending on the desired density function across the aperture. In each transmission-reception process, both apertures are randomly selected according to their respective density function, thereby increasing the diversity of the diffraction pattern. Figure 3 presents an example of the solutions adopted for transmission (left) and reception (right) and the corresponding element density distributions.

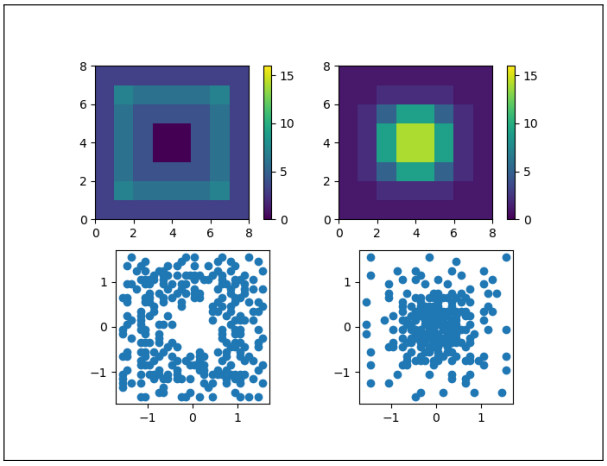

Figure 3. The 256 sparse array distribution. Top: In the left, element density for reception aperture. In the right, element density for transmission aperture. Bottom: In the left, example of reception aperture. In the right, example of transmission aperture.

For analyzing the process of generating an image for a single deflection angle (0^o) and compare the image from the full array with the one obtained using the sparse aperture, we have simulated the position of a line of scatterers along the Z-axis, separated by $0.25mm$. To assess the effect caused by diffraction, no white noise has been introduced into the model.

In Figure 4, we present the result of the full aperture. The image exhibits a large number of lobes and artifacts. To generate the final image, this image is combined with others obtained at different transmission angles, thereby reducing the interference pattern.

In Figure 5, we present the result of the sparse aperture. The image exhibits a significant reduction in artifacts, a lateral resolution comparable to that of the full aperture, and a secondary lobe pattern characteristic of the ring-shaped aperture.

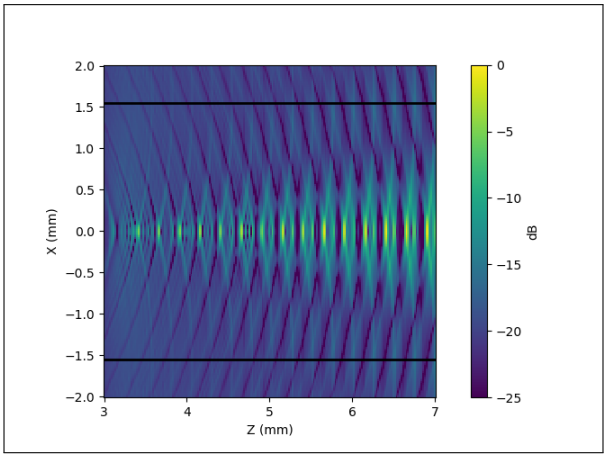

Figure 4. Image produced in the plane of interest ($Y = 0$) by the full aperture.

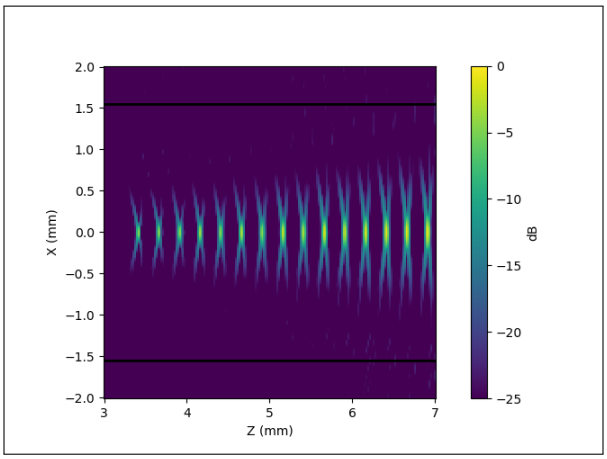

Figure 5. Image produced in the plane of interest ($Y = 0$) by the sparse aperture configuration.

To understand how the complete process works, we designed a sampling scheme with up to 32 emission shots, oriented to cover the entire reference volume. The scanning strategy follows a Fermat distribution based on the golden angle [8]. For the conventional plane-wave image, where emission superposition occurs in the illuminated scene, the final image is obtained by averaging the

32 steered images. To evaluate this process, we considered a more complex scene composed of a set of reflectors distributed in the XZ plane, maintaining the distribution along Z and a constant angular distribution along X. Figure 6 illustrates this in the case of a full aperture. The image can capture the presence of the reflectors but exhibits very low contrast.

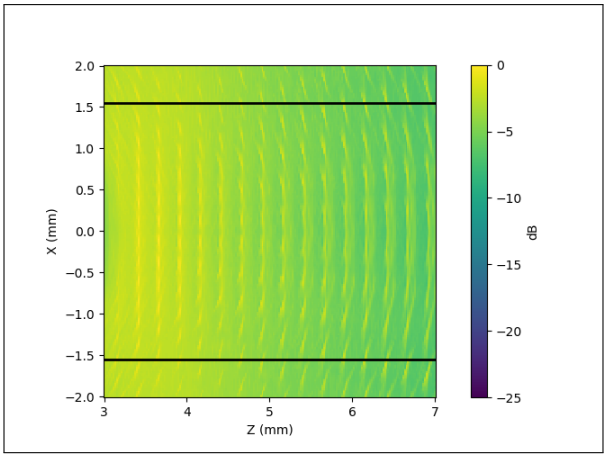

Figure 6. Image produced in the plane of interest ($Y = 0$) by the full aperture.

In the case of the proposed technique based on sparse apodized apertures, averaging between images cannot be applied since the emission beams are narrower and the images have minimal overlap. Therefore, the contribution of each image must be weighted according to the degree of influence that the emission beam has on the point under study. As explained earlier, while maintaining each aperture's respective density function for each shot, two new apertures are randomly generated—one for transmission and one for reception.

This operating approach, using sparse apertures and plane waves, offers an interesting alternative for integrating signal averaging. For a given angle, once a reception aperture has been selected, we could perform multiple consecutive transmissions with different sparse transmission apertures. By maintaining the same transmit lens and the same reception aperture, the signals can be directly averaged in the acquisition buffer.

By considering multiple sparse apertures for transmission that share the same main wavefront but produce different interfering secondary wavefronts, we can reinforce the main wavefront while generating destructive interference for the secondary wavefronts, thus minimizing their contribution to image artifacts (see figure 7). By adjusting the interference based on the relationship between transmission timing and time-of-flight, it is possible to make these variations "transparent" to the system, especially if a dual-buffer system is implemented.

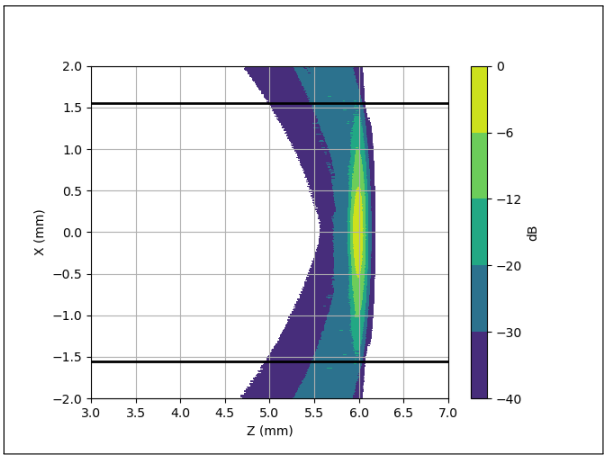

Figure 7. Emission waveform in $Y = 0$ averaged by 16 sparse apertures with 256 elements, following a density apodization based on Taylor window

Therefore, during the emission time of 32 shots required to obtain these 32 images, a total of 544 dispersed apertures were generated (32 for reception and 32×16 for transmission). The image produced by this configuration for the proposed imaging region is shown in Figure 8. Compared to the full-aperture image, the sparse array image improves contrast while maintaining lateral resolution. Residual secondary lobes are still present, but they are not significant enough to degrade image quality.

2.1 Volumetric imaging

We now consider a three-dimensional scene in which the reflectors are distributed along a spiral cone, with its vertex located at the center of the aperture. In this configuration, the reflectors are positioned at varying angles in both elevation and azimuth, as well as at different radial distances within the scanning volume. This setup allows us to compare the imaging performance of a full array versus a sparse array. In both apertures, the 32-angle sampling strategy based on the Fermat spiral was used. The figures display isosurfaces at -12 dB levels. To enhance the interpretability of the scene, the maximum intensities have been projected onto the XY, XZ, and YZ planes.

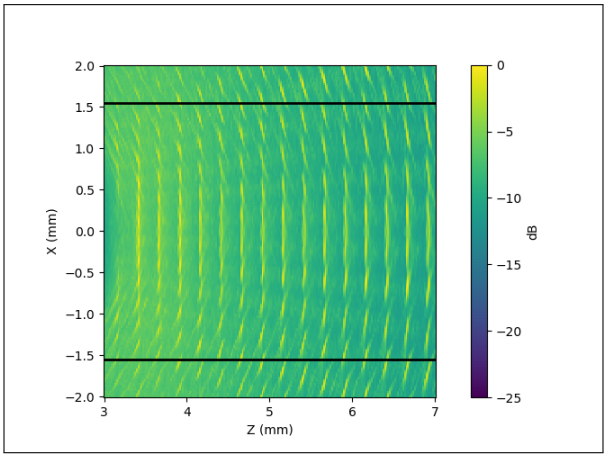

Figure 8. Image produced by the sparse aperture in the plane of interest ($Y = 0$). 16 averaged emissions performed.

The image obtained using the full aperture (Figure 9) exhibits limited dynamic range and resolution, indicating that the proposed scan is not sufficiently dense to produce a high-quality image. In contrast, the image generated using the sparse aperture—by introducing averaging and performing 16 transmissions (each with a different sparse emission aperture) per reception aperture—shows a significant improvement in dynamic range, along with a slight enhancement in lateral resolution compared to the non-averaged approach (Figure 10).

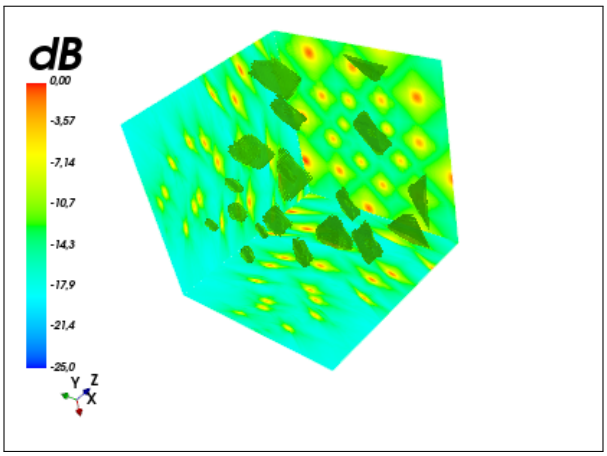

Figure 9. Volumetric image produced by the Full aperture.

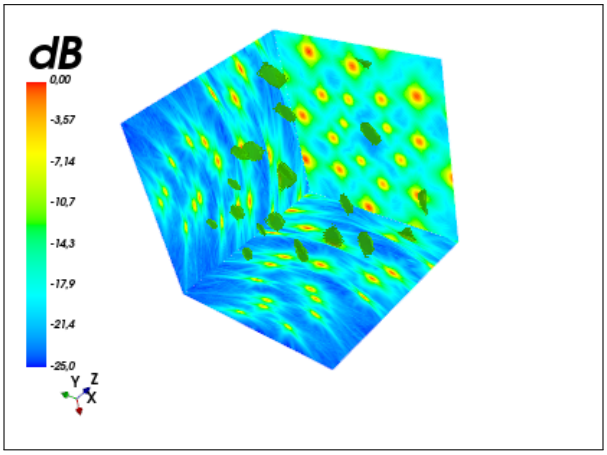

Figure 10. Volumetric image produced by the sparse aperture. 16 averaged emissions performed

The comparison between both apertures demonstrates that, when properly organized, sparsity can be effectively exploited to enhance near-field aperture performance and yield high-quality images. Averaging over the acquisition channels enables this process without incurring additional data flow costs. Furthermore, if the system supports double buffering for acquisitions and allows synchronization of the averaging transmissions with the transmit timing, the process can be rendered effectively transparent in terms of acquisition time. Within this imaging range and under plane wave illumination, the full aperture introduces a substantial number of artifacts and requires greater angular diversity and a higher number of transmissions to achieve comparable image quality.

3. CONCLUSIONS AND FUTURE WORK

The work has proposed a strategy for using sparse apertures in a plane-wave imaging system. Instead of proposing an exhaustive search for a solution, an open approach has been taken, where dozens of apertures are utilized to exploit the diversity they offer in order to improve the overall image result, according to a spatial distribution pattern designed to achieve a specific apodization response. In a way, the apodization used narrows the beam during emission, which nonetheless remains wide enough to allow for a sweep with a narrow beam during reception, generating a type of multi-beam focusing. It has been demonstrated how we can use several sparse apertures in transmission for the same reception to improve the signal-

to-noise ratio, and it has been suggested how this process can be integrated into the system as an averaging operation, parallelizing its activity with data transmission to maintain the acquisition rate at the desired values.

To evaluate this, three possible scenarios were designed in which we could compare the improvement relative to the flat aperture case. On one hand, the reduction of the artifact pattern caused by multiple wavefronts generated in the near field. On the other hand, the improvement in dynamic range when the interfering pattern becomes more complicated due to the regularity of the reflectors. And finally, when the volumetric image as a whole is considered. In all of these scenarios, the sparse aperture image has maintained an excellent response in terms of lateral resolution, even improving upon that of the full aperture.

The proposal is aligned with the objectives of the project, which seek to enhance the detection of microstructures using plane wave high-frame-rate imaging, while simultaneously reducing computational complexity and adapting the sensor to the available hardware resources. The forthcoming development of this work is directed toward the experimental phase, with the aim of assessing the performance of this technique when applied to functional imaging.

4. ACKNOWLEDGMENTS

Jorge Huecas, Staff hired under the Generation D initiative, promoted by Red.es, an organisation attached to the Ministry for Digital Transformation and the Civil Service, for the attraction and retention of talent through grants and training contracts, financed by the Recovery, Transformation and Resilience Plan through the European Union's Next Generation funds.

This research work was funded by the European Commission – NextGenerationEU, through Momentum CSIC Programme: Develop Your Digital Talent

This research work was funded by: PID2022 - 138013OB -I00 /MCIN /AEI /10.13039/ 501100011033/ FEDER, UE

This work has been developed within the framework of the LUNABRAIN-CM project, funded with €1,026 million by the Community of Madrid through the R&D activities program in technologies, granted by Order 5696/2024

5. REFERENCES

[1] Montaldo, G., Tanter, M., Bercoff, J., Benech, P., and Fink, M. Coherent plane-wave compounding for very high frame rate ultrasonography and transient elastography. In *IEEE Transactions on Ultrasonics, Ferroelectrics, and Frequency Control*, 56(3), 489–506, 2009.

[2] Heiles B, Correia M, Hingot V, Pernot M, Provost J, Tanter M, Couture O. Ultrafast 3D Ultrasound Localization Microscopy Using a 32 × 32 Matrix Array *IEEE Trans Med Imaging*, 38(9):2005-2015. doi: 10.1109/TMI.2018.2890358. 2019.

[3] Chavignon A, Heiles B, Hingot V, Orset C, Vivien D, Couture O. 3D Transcranial Ultrasound Localization Microscopy in the Rat Brain With a Multiplexed Matrix Probe. *IEEE Trans Biomed Eng*. 69(7):2132-2142. doi: 10.1109/TBME.2021.3137265. 2022.

[4] Zhang C, Lei S, Ma A, Wang B, Wang S, Liu J, Shang D, Zhang Q, Li Y, Zheng H, Ma T. Evaluation of tumor microvasculature with 3D ultrasound localization microscopy based on 2D matrix array. *Eur Radiol*. 34(8):5250-5259. doi: 10.1007/s00330-023-10039-x. 2024.

[5] Li X, Gachagan A, Murray P. Design of 2D Sparse Array Transducers for Anomaly Detection in Medical Phantoms. *Sensors*. 20(18):5370. doi: 10.3390/s20185370. 2020

[6] Martínez-Graullera Ó, de Souza JCE, Parrilla Romero M, Higuti RT. Design of 2D Planar Sparse Binned Arrays Based on the Coarray Analysis. *Sensors*. 21(23):8018. doi: 10.3390/s21238018. 2021

[7] Maffett R, Boni E, Chee AJY, Yiu BYS, Savoia AS, Ramalli A, Tortoli P, Yu ACH. Unfocused Field Analysis of a Density-Tapered Spiral Array for High-Volume-Rate 3-D Ultrasound Imaging. *IEEE Trans Ultrason Ferroelectr Freq Control*. 69(10):2810-2822. doi: 10.1109/TUFFC.2022.3188245. 2022

[8] J.N. Ridley, Packing efficiency in sunflower heads, *Mathematical Biosciences,* Volume 58, Issue 1, Pages 129-139, ISSN 0025-5564, https://doi.org/10.1016/0025-5564(82)90056-6. 1982,